

Investigation of adsorption of metronidazole on Chitosan - Halloysite nanocomposites and controlled release

Merve Öztekin¹ & Yeşim Sağaçık^{1*,2}

¹Hacettepe University, Bioengineering Division, Institute of Science, 06800, Beytepe, Ankara, Turkey

²Hacettepe University, Chemical Engineering Department, 06800, Beytepe, Ankara, Turkey

E-mail: yesims@hacettepe@edu.tr

Received 12 November 2018; accepted 30 January 2020

A novel nanocomposite drug carrier composing from chitosan (CTN) and halloysite nanotubes (HNTs) has been developed. For this purpose, the metronidazole (MNZ) is chosen as a model drug. The characterization of synthesized nanocomposites is performed by FTIR, TGA, DSC, SEM, TEM, BET and particle size distribution analysis. MNZ is loaded to chitosan-halloysite (CTN-HNT) nanocomposites in two ways; by direct loading and adsorption method. The adsorption of MNZ on CTN-HNT nanocomposites has been investigated as a function of medium pH, mass ratio of CTN to halloysite (HNT), amount of nanocomposite and drug concentration. The fit of MNZ adsorption equilibrium on CTN-HNT nanocomposites to the Langmuir and Freundlich models was investigated. The adsorption kinetics of MNZ on nanocomposites have been evaluated using the pseudo-first order rate equation of Lagergren and the pseudo-second-order rate equation of Mc-Kay and Ho. The controlled release of MNZ from CTN-HNT nanocomposites has also been investigated.

Keywords: Adsorption, Chitosan-Halloysite nanocomposite, Drug carrier, Metronidazole, Sustained release

The use of novel natural biopolymer-clay nanocomposites as drug carrier systems has received great attention in the last few years. Chitin, the main component of the cell walls of fungi, the exoskeletons of arthropods such as crustaceans and insects is a long-chain biopolymer of N-acetylglucosamine and is the second abundant biopolymer in nature after cellulose¹. Chitosan (CTN) which is obtained by alkaline deacetylation of chitin is a linear polysaccharide composed of randomly distributed β -(1-4)-linked D-glucosamine and N-acetyl-D-glucosamine². Due to its intrinsic bio-friendly properties, good biocompatibility, biodegradability and abundant availabilities, CTN biogel beads and films have been used in the fields of biomedical and pharmaceutical, i.e. artificial skin, wound dressing tissue engineering, drug carrier, and water treatments, cosmetic and so on. However, the mechanical and thermal properties of CTN should be improved for wider applicability in these fields³. Various types of materials as micro and nanofillers, such as silica, hydroxyapatite, calcium phosphate, nanoclay, organo modified montmorillonite, carbon nanotubes, titanium dioxide, graphene have been incorporated for reinforcing CTN⁴. Nevertheless, the synthesis, incorporation and functionalization of all these fillers

are expensive and complex processes that require the use of too many chemical materials. CTN has amino and hydroxyl groups and is positively charged due to the protonation of the amines in acidic solutions below pH 5.0. For that reason, hydrogen bonding and/or electrostatic attraction interactions play an important role interactions of CTN with nanoclays⁵.

HNTs with a chemical formula of $\text{Al}_2\text{Si}_2\text{O}_5(\text{OH})_4 \cdot n\text{H}_2\text{O}$, excellent tubular microstructure and high mechanical and thermal strength, can be used to prepare the CTN nanocomposites⁶. HNTs are a dioctahedral 1:1 clay mineral that generally exist in soils and have dominantly hollow tubular structure⁷. Due to the hydrophilicity and small dimensions of HNTs, natural HNTs are readily dispersed in water by ultrasonic treatment or mechanical stirring, which is convenient to mix with CTN in aqueous solution for preparing nanocomposite⁸. The zeta-potential of HNTs was recorded to be negative at pH 2-13. The chemical properties of HNTs' outer surface are similar to those of the negative SiO_2 , while the properties of the inner cylinder are similar to those of the positive Al_2O_3 ⁹. The crystalline multilayer tube wall of HNT consists of a corner-shaped tetrahedral SiO_2 sheet stowed with an edge-shared octahedral AlO_6 sheet with an internal aluminol group Al-OH. Different

chemical composition and charge of inner and outer surfaces of HNTs makes their selective lumen modification easy¹⁰. While HNT readily adsorbs polycations to form nanocomposites, inner lumen of the HNT can store and release molecules in a controllable manner, making these nanoreactors attractive for applications in self-healing polymeric composites, drug delivery and regenerative medicine.

The HNTs can be used as reinforcing filler for biopolymers as well as carriers for the controlled release of antioxidants, flame-retardants, corrosion inhibitors, biocides, drugs, DNA, proteins and quantum dots¹¹. The adsorption of biopolymers, anionic pectin, cationic CTN and neutral hydroxypropyl cellulose onto HNTs, and the thermodynamic and surface properties of the HNT dispersed in aqueous solutions of these biopolymers were investigated¹². Pectin as a matrix and HNTs as a reinforcer were used to prepare bionanocomposite films for food packaging applications. The release kinetics of pectin-HNT bionanocomposites was investigated by encapsulating salicylic acid as a biocidal agent into the lumen of HNTs¹³. Mechanical performances, thermal stability and wettability of CTN, methylcellulose and alginate matrixes filled with HNTs were investigated. The interaction of the cationic polymer CTN was shown to occur with the negative outer surface of the HNT and that of the anionic alginate with the inner surface of the cavity having positive charge. However, a nonionic polymer methyl cellulose interacted without specificity with the inner and outer surfaces of HNTs¹⁴. Inorganic reverse micelles based on HNTs and hexadecyltrimethylammonium bromides were prepared. The HNTs were dispersed in chloroform to encapsulate aqueous sodium alginate and calcium chloride into their lumen. Doxycycline was used as a model drug for loading and release from the Ca²⁺-crosslinked alginate inside the HNT hydrophilic lumen¹¹. Among the tested matrix and filler systems, the most suitable bionanocomposite for the sustained drug release in the gastrointestinal (GI) tract seems to be CTN-HNTs. When HNTs are mixed with CTN in dilute acidic solution, CTN-HNT nanocomposites are formed mainly via electrostatic attractions. The amino-group and hydroxyl groups of CTN also form hydrogen bonds with the Al-O-H and silanols on the surfaces of HNTs. The hydrogen bonding and electrostatic interactions between HNTs and CTN make available for interfacial binding¹⁵. CTN has good

interfacial compatibility with HNTs, which improves dispersion of HNTs in CTN solution. The eco-friendly, biocompatible, available abundant and mechanically strong nature of HNTs make them an important-alternative nanomaterial for developing new CTN nanocomposites.

Nitroimidazole antibiotics are used to treat parasitic infections, amoebiasis, bacterial vaginosis, gastrointestinal infections, skin infections, meningitis, lower respiratory infections, bacterial infections, diarrhea, and rosacea. Nitroimidazoles are among the most extensively manufactured and written out a prescription antibiotics in many countries. This drug family is mutagenic, carcinogenic, and has high solubility in water, high toxicity, and low biodegradability. In sewage treatment plants, these antibiotics have been measured at mg L⁻¹ concentration levels. Nitroimidazole antibiotics compose of three drugs. These include metronidazole (MNZ), tinidazole and nimorazole. MNZ is an inexpensive drug used to treat certain kinds of bacterial and protozoal infections. This drug is more popular than comparable drugs. It is used to treat bacterial infections of the vagina, stomach, skin, joints and respiratory tract¹⁶. MNZ is an active supplement in the treatment of *H. pylori*, which causes anorexia, nausea, vomiting, and epigastric pain¹⁷.

One of the aims of novel biopolymer-clay nanocomposites as drug carriers is to prolong the residence time of drug in the GI tract. A continuous layer of insoluble mucus hydrogel coats the whole GI tract including the stomach¹⁸. The mucus hydrogel layer consisting of glycoproteins; due to their content of ester sulfate and sialic acid groups has a vigorous net negative charge. Mucoadhesive drug release systems increase the drug residence time at the site of desorption or re-adsorption¹⁹. Biopolymers with high charge density work as good mucoadhesive agents. The adhesive properties of CTN in a swollen state continue well during repeated contacts of CTN and the mucosal tissues. The ionic interactions between the positively charged amino groups of CTN and the negatively charged mucus gel layer are perhaps the most important reasons for the attachment to the mucosal layer. In addition to ionic interactions, the adhesion by hydration and hydrogen bonding might have been involved in the interaction mechanisms. Due to the adherence of CTN layer on HNTs to the mucosal tissues, the residence time of drug enhances and the bioactive agent is absorbed on the active sites of surfaces. Hydrophilic nanocomposites based on

CTN-HNTs can control the rate of drug release and diffusion, prolong the time of the therapeutic effect, distribute the drug to specific sites in the body, improve drug bioavailability and effectiveness²⁰.

For this purpose, the MNZ from the nitroimidazole family was chosen as a model drug. MNZ was loaded to CTN nanoparticles directly for drug delivery application previously²¹. In this study, it was aimed to obtain the adsorbent material with superior properties than the two components by making the nanocomposites of CTN with HNTs via solution mixing and freeze-drying techniques. With respect to our knowledge, MNZ has just been loaded to CTN-HNT nanocomposites via adsorption for the first time in the literature. Various parameters affecting the MNZ adsorption process such as pH, the mass ratio of HNT to CTN, amount of nanocomposite and MNZ concentration have been investigated. MNZ release property of CTN.

HNT nanocomposites in phosphate buffered saline (PBS) simulating the intestine tract has been researched.

Experimental Section

Materials

The HNTs (CAS No: 1332-58-7) and CTN powder (CAS No: 9012-76-4) with low molecular weight (%75-%85 deacetylated) were purchased from Sigma-Aldrich. Deionized (DI) water obtained from Thermo Scientific Smart2Pure water purification system, with resistivity of 18.2 M Ω cm was used for preparation of all solutions. MNZ (CAS No: 443-48-1), acetic acid, hydrochloric acid, potassium phosphate monobasic (KH₂PO₄) were supplied from Sigma-Aldrich.

Preparation of HNT-CTN nanocomposites

HNTs were dissolved in 100 mL deionized water, 1% (w/v) HNTs solution was homogenized in ultrasonic bath for 1 h. CTN (0.5 g) was dissolved in 100 mL of 1% (wt/v) acetic acid solution until the solution became clear. CTN (0.5% (wt/v) solution was added to the homogenized HNT solution. The mixture was stirred for 24 h on a magnetic stirrer and then centrifuged. The supernatant liquid was poured and, the precipitated CTN-HNT, to remove excess CTN and acetic acid, was washed with deionized water till pH 7.0. The CTN-HNT nanocomposites were lyophilized at -50°C using a Christ freeze dryer. The concentration of free CTN in the supernatant liquid and washing-deionized water was determined spectrophotometrically²². The blue-coloured complex

of CTN with bromocresol purple was measured using Genesys 10s UV-Vis spectrophotometer at 589 nm.

Characterization of HNT-CTN nanocomposites

Fourier Transform Infrared (FTIR) spectroscopy

FTIR was used to understand the chemical composition of the pure CTN, HNT and CTN-HNT nanocomposites. Chemical interactions between CTN and HNT were analysed comparing the chemical structure of CTN-HNT with the bare CTN and HNT. The FTIR spectra of the freeze-dried CTN-HNT samples were measured using attenuated total reflectance (ATR) model using Thermo Scientific Nicolet 6700. Thirty-two consecutive scans were taken and their average was recorded. Spectra were taken from 4000 to 400 cm⁻¹. The resolution of the wavenumber was 4 cm⁻¹.

Thermogravimetry (TGA) and Differential Scanning Calorimetry (DSC) analysis

Freezing-dried samples of blank CTN, HNT and CTN-HNT nanocomposites were used in thermogravimetric analysis. TGA and DSC analyses were performed with powder samples under N₂ gas flow rate of 200 cm³ min⁻¹ using SII EXSTAR 6000 TG/DTA 6300 TGA and Perkin Elmer Diamond DSC. In TGA, 10 mg samples of blank CTN, HNT and CTN-HNT nanocomposites were heated from 30°C to 700°C at a heating rate of 10°C min⁻¹ in N₂. In DSC, the temperature range in which the samples were heated ranged from 0°C to 500°C.

Measurement of distribution of nanocomposite size

The size distribution profiles of the CTN-HNT nanocomposites in a suspension were measured by a Malvern Mastersizer 2000 (Malvern Instruments Ltd., UK). Mastersize device which measure the size of particles ranging from 20 nm to 2 mm is based on Mie theory. The reflected and broken laser light from sample is measured by detectors. The angle and intensity of the scattered light determine the particle size distribution. The scattering angle of the laser beam passing through the particle depends on the particle size.

Scanning Electron Microscopy (SEM)

Before SEM observation, the CTN-HNT nanocomposites were coated with 2 nm thick gold-palladium using a sputter coated. The morphology of CTN-HNT nanocomposites was investigated by Quanta 400F field emission scanning electron microscopy.

Transmission Electron Microscopy (TEM)

The powdered samples were placed in eppendorf tubes with an appropriate solvent. The amount of solid sample in the suspension should be between 0.1% and 1%. The solid sample in suspension was kept in an ultrasonic water bath until it is completely homogeneously dispersed. Care must be taken to avoid visible pellets. The 400 mesh carbon-coated copper grid was held with tweezers and fixed. 3-5 μL of the resulting suspension was dropped on the carbon-coated grid fixed with a micropipette by 3-5 μL . The substance placed on the carbon-coated grill was expected to dry completely. Then the samples were observed using a FEI Tecnai G² Spirit Bio (TWIN) high contrast transmission electron microscope under accelerating voltage of 120 kV.

Brunauer-Emmett-Teller (BET) measurements

The BET analysis was primarily performed to obtain a sample surface area, pore size distribution, and pore shape. Measurements can be made on pellets, dust and solid pieces. The samples must be preheated at 150°C for 2 h under vacuum to remove adsorbed water, moisture or other volatile materials. At least 5 g of sample should be provided for the measurement. N₂ gas was used during the analysis. Multi-point BET area and pore size distribution analyzes were performed on the CTN-HNT samples by Surface Characterization Device Quantachrome Corporation, Autosorb-6B.

MNZ adsorption studies on CTN-HNT nanocomposites

MNZ adsorption studies on CTN-HNT nanocomposites were performed in an orbital agitated incubator operated at 175 rpm and at 25°C, while the volume of batches was 100 mL. Before beginning adsorption experiments, initial pH of MNZ solutions were adjusted to the required values using 0.1 M and 1.0 M NaOH and HCl solutions. Samples taken from the adsorption media at certain time periods of 0.5, 15, 30, 60, 120, 180 and 1440 mins were centrifuged at 19,000 g for 10 min. using a Hermle Z300 centrifuge. The concentration of free MNZ in the supernatant liquid was measured using Genesys 10s UV-Vis spectrophotometer at 320 nm.

MNZ loading to CTN-HNT nanocomposites

The MNZ loading to the CTN-HNT nanocomposites was performed by adding the drug to the HNTs solution, with a HNTs to MNZ ratio of 10:1. 3 g of HNTs and 0.3 g of MNZ were dissolved in 100 mL of 0.5% (v/v) acetic acid solution and this

solution was stirred on the magnetic stirrer for 24 h. 1 g of CTN was weighed and dissolved in 100 mL of 1% (v/v) acetic acid solution and this solution was added to the HNT/MNZ solution. The final solution was kept waiting on the magnetic stirrer for 24 h, and then was centrifuged for 45 min at 4°C using Hettich Universal 320R refrigerated centrifuge. The MNZ loaded CTN-HNT nanocomposites were washed with deionized water to remove the solvents and were freeze-dried for 24 hours using Christ freeze-drier.

MNZ release from CTN-HNT nanocomposites

10 mg MNZ loaded CTN-HNT nanocomposite was added to 100 mL of 0.1 M Phosphate-Buffer Solution (PBS) at pH 7.4 in the orbital shaker operated at 37°C. Samples taken from the media at certain time periods of 0.5, 15, 30, 60, 120, 180 and 1440 min were centrifuged at 19,000 g for 5 min. using a Hermle Z300 centrifuge. The concentration of released MNZ in the PBS was measured using Genesys 10s UV-Vis spectrophotometer at 320 nm.

Results and Discussion

Characterization of CTN-HNT nanocomposites

FTIR spectroscopy

To explore the interactions between CTN and HNTs, FTIR spectra for the pure CTN, HNTs and CTN-HNT nanocomposites were compared (Fig. 1). Both the characteristic peaks of pure CTN and that of HNTs were observed in the FTIR spectra of CTN-HNT

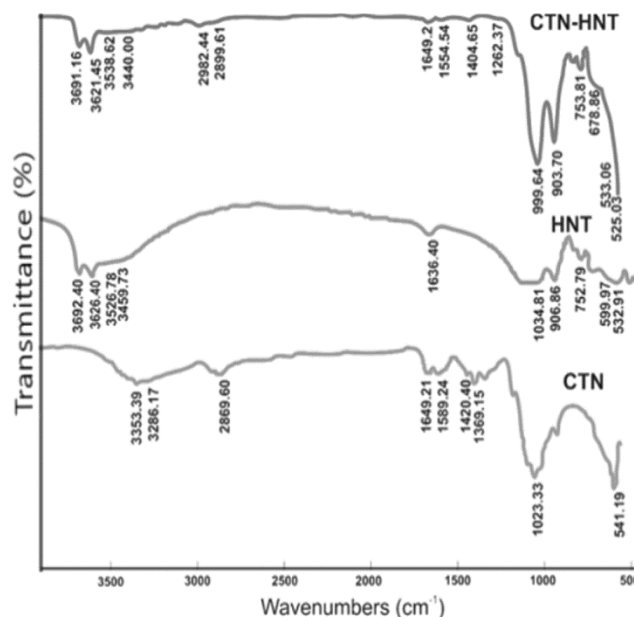


Fig. 1 — Fourier Transform Infrared (FTIR) spectra of CTN-HNT nanocomposite, pure HNT, pure CTN from top to bottom, respectively.

nanocomposites. It was pointed out that CTN was successfully incorporated with HNTs. Characteristic peaks including O-H stretching of water 3459 cm^{-1} , O-H deformation of water 1636 , in-plane Si-O stretching 1034 cm^{-1} were observed in the infrared spectrum of pure HNTs²³. The stretching vibrations of hydroxyl groups at the surface of HNTs gave the characteristic double peaks at 3692 and 3625 cm^{-1} . The pK_a of CTN is around 6.2, CTN is positively charged in solution below pH 5.0 due to the protonation of the amines. On the contrary, HNTs are negatively charged due to isomorphous substitution of Al^{3+} for Si^{4+} . For that reason, electrostatic attractions play an important role in coating of HNTs with CTN. The intensity loss of the band at 3691 and 3621 cm^{-1} in the FTIR spectrum of CTN-HNT nanocomposites was due to the electrostatic interaction of the positively charged amino groups of CTN with the negatively charged sites of the HNTs. Besides the amine groups and hydroxyl groups on the CTN are in interaction with the Si-O bonds and/or hydroxyl groups of HNTs through hydrogen bonding interactions. The existence of hydrogen bond interactions between CTN and the silicate surface of HNTs was also proven with IR spectroscopy. The two peaks around 1034 and 906 cm^{-1} for pure HNTs are ascribed to in-plane Si-O stretching and O-H deformation of inner hydroxyl groups. These peaks shifted to lower wavenumbers from 1034 to 999 cm^{-1} and from 906 to 903 cm^{-1} in the CTN-HNT nanocomposites. The hydrogen bonding interactions between HNTs and CTN are responsible for this shift²⁴. The absorption peaks at 599 and 532 cm^{-1} were due to perpendicular Si-O stretching and deformation of Al-O-Si, respectively. These peaks decayed in the FTIR spectrum of CTN-HNT nanocomposites. Because the protons in CTN are hydrogen-bonded to the oxygen species of Si-O and Al-O segment, Si-O and Al-O bonds weakened and the tetrahedral symmetry of these parts deformed. The bands observed at 3526 and 3459 cm^{-1} of HNTs spreaded with intensity loss in CTN-HNT nanocomposites. The O-H stretching frequencies of the CTN-HNT nanocomposites shifted to 3538 and 3440 cm^{-1} . It may be attributed to formation hydrogen bonds between the lattice hydroxyls and organic groups.

The characteristic peaks seemed in the FTIR spectrum of pure CTN were vibration of OH groups at 3353 and 3286 cm^{-1} , C-H bond ($-CH_3$) at 2869 cm^{-1} , carbonyl bonds ($C=O$) of amide groups $C=O-NHR$ at 1649 - 1420 cm^{-1} . The peak around 1023 cm^{-1} of pure

CTN represents the vibration of the C-O bond. Two characteristic peaks at 1589 and 1420 cm^{-1} observed in the spectrum of pure CTN correspond to the deformation vibration of the protonated amine group ($-NH_3^+$) and hydroxyl group, respectively. The two peaks of the CTN-HNT nanocomposites shifted and spreaded out were the absorbance bands of NH_2 and OH vibrations observed between 1404 and 1554 cm^{-1} . Compared to the raw sample of HNTs, some new peaks at 1649 and 1554 cm^{-1} referring amide I and II groups of CTN were observed in the FTIR spectrum of CTN-HNT nanocomposites. The broad peaks around 3286 - 3353 cm^{-1} of CTN are ascribed to the overlapped N-H band and O-H band vibration. These peaks moved to higher frequencies around 3440 cm^{-1} in CTN-HNT nanocomposites. All the changes observed in FTIR spectrum of CNT-HNTs nanocomposites indicated that the interactions between HNTs and CTN occurs via the electrostatic interaction and hydrogen bonding.

TGA analysis

The thermal stability behavior of CTN-HNT nanocomposites show differences from pure CTN and HNTs (Fig. 2). The main two phases of decomposition of CTN were observed at around 60 and 244°C in the TGA curves, which are corresponded to the loss of free water and the degradation of the CTN chains, respectively. The first weight loss thought to be due to moisture vaporization corresponded to 9.3% loss in weight. The second weight loss beginning at around 244°C was about 33.7%, which is attributed to the decomposition of CTN. The total weight loss of pure CTN was 47.6% at about 500°C . For pure HNTs, the

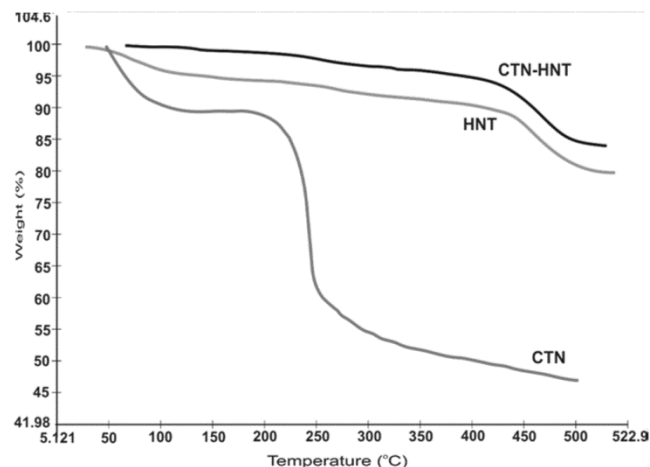


Fig. 2 — Thermogravimetric analysis of CTN-HNT nanocomposite (TGA), pure HNT, pure CTN from top to bottom, respectively.

first endothermic peak was observed at 77.7°C. This is thought to be due to vaporization of adsorbed water and the first weight loss was 3.2%. The second endothermic peak observed at 271 °C was the result of the removal of water in the inside layers or lumens of pure HNTs and the corresponding weight loss was 2.2%. Only one peak ascribed to the structural dehydroxylation caused by the separation of the OH ions in the clay layers of pure HNTs was obtained at around 488°C in the TGA curves. The corresponding weight loss was recorded as about 11.4% and the total weight loss at about 500°C was 18.6%. In the CTN-HNT nanocomposites, two peaks were observed at around 256 and 484°C, which are assigned to the degradation of CTN and HNTs, respectively. The matching weight losses were measured as 2.9% and 11.8%, respectively. It was seen from the TGA curves that the thermal decomposition temperature of HNTs component in the CTN-HNTs nanocomposites was slightly decreased from 488°C to 484°C compared to pure HNTs, while the degradation temperature of CTN

component was slightly increased from 244 to 256°C compared to raw CTN. When HNTs were added to CTN, the thermal stability of CTN-HNT nanocomposites increased drastically and approached the thermal stability of pure HNTs. Char residue of CTN-HNT nanocomposites constitutes a barrier and obstruct the volatile escape while contributing to enhance the thermal stability. As HNTs lumens have high volume percentages, significant amounts of degraded products of CTN may be entrapped within the lumens of HNTs. For that reason, diffusive mass and heat transport can be delayed in some degree in the CTN-HNT nanocomposites.

DSC analysis

The thermochemical behavior defined by the DSC curves was consistent with that indicated by the TGA curves (Fig. 3). The DSC curve of pure CTN showed an endothermic peak centered at around 75°C, which is referred to the loss of water associated with the

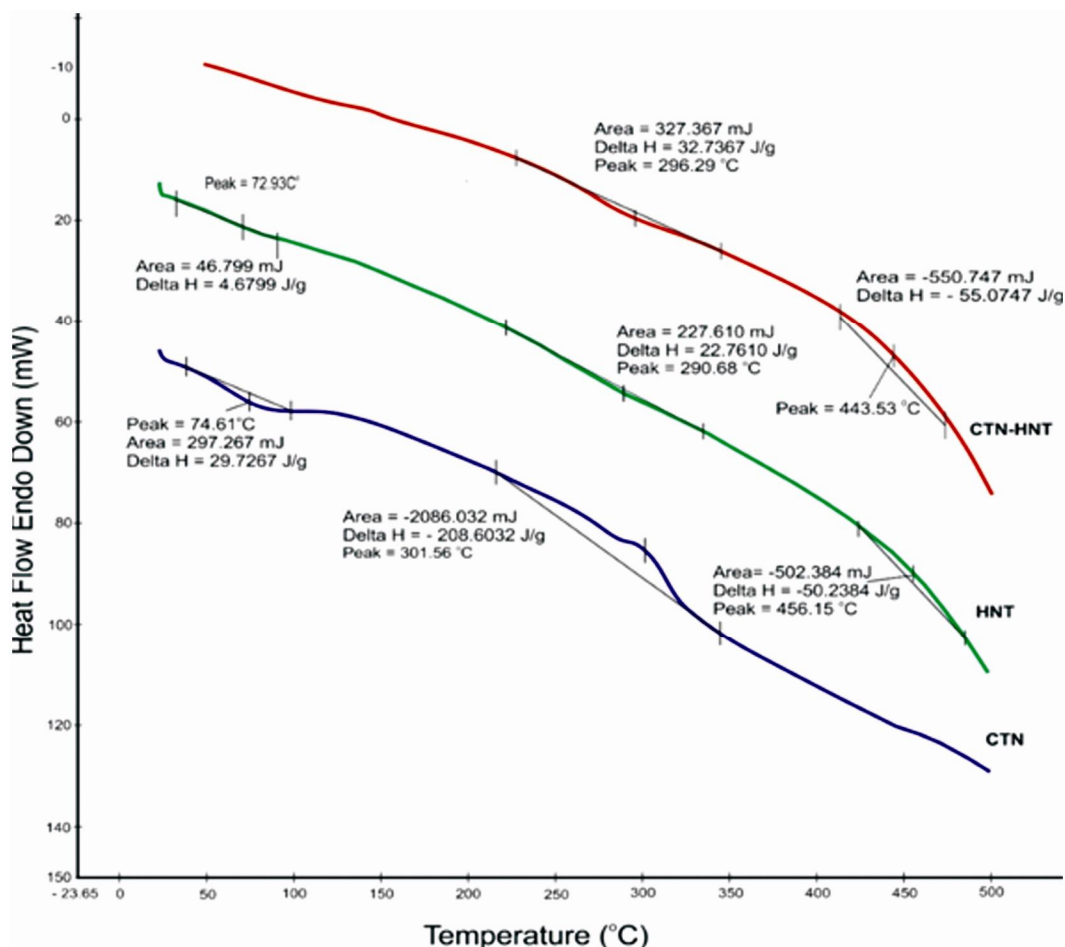


Fig. 3 — Differential scanning calorimetry analysis (DSC) of CTN-HNT nanocomposite, pure HNT, pure CTN from top to bottom, respectively.

hydrophilic groups of polymer. The broad exothermic peak which appeared in the temperature range between about 250 and 350°C and centered at around 302°C indicated the degradation of the pure CTN. Three stages of DSC curves for pure HNTs were observed at around 73, 291 and 456°C, which were assigned to the loss of adsorbed water, removal of water in the inside layers or lumens, and the structural dehydroxylation of HNTs, respectively. In the DSC curves of CTN-HNT, two peaks were obtained at around 296 and 444°C, which were specified as the degradation of CTN, and HNTs, respectively.

Particle size distribution analysis

The hydrodynamic sizes of CTN-HNT nanocomposites and HNTs suspended within a dispersion medium were measured using Mastersizer. The average size of HNTs was measured as 348 nm. The average size of CNT-HNT nanocomposites was detected to be 664 nm (Fig. 4). Synthesized CNT-HNT nanocomposites have usually broad and partially non-uniform size distribution. To prevent the sticking of the nanocomposites which determine the average size distribution by particle size distribution analysis, freeze-drying procedure was not applied. The suspended CTN-HNT nanocomposites were sonicated for 5 min before analysis. If particle size distribution analysis time is kept longer than necessary, CTN-HNT nanocomposites in the dispersion medium combine to form nano agglomerates. This causes the sizes of the nanocomposites to be measured larger than they are.

SEM analysis

According to SEM images, HNTs are seen as three-dimensional (3D) nanotubes and they have cylindrical-shaped tubular morphology (Fig. 5 a). Tubular structure of HNT is clearly distinguished in the SEM images. According to the SEM images, the diameters of pure HNTs ranged from 66 nm to

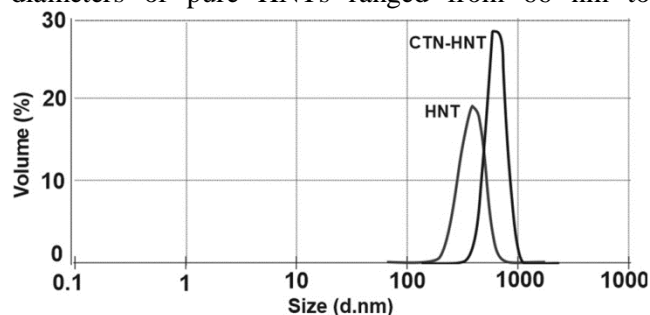


Fig. 4 — Particle size distribution analysis diagram of synthesized pure HNT and CTN-HNT nanocomposite.

169 nm, while their lengths changed from 404 nm to 577 nm. The tube walls of raw HNTs seem to be clean and smooth, however, the walls of CTN-HNT nanocomposites are rough and indistinct. The edge of HNT also appears to be clear and sharp. Compared to natural HNT, the tube wall of HNT formed nanocomposite with CTN becomes thicker and rougher because of CTN coating (Fig. 5 b,c,d). As inner lumens and pores of HNTs filled with CTN and outer surface coated with CTN, the tube walls of CTN-HNT nanocomposites are seem to be thicker. The diameters of CTN-HNT nanocomposites were observed to vary between 82 nm and 250 nm while their lengths ranged from 440 nm to 778 nm.

HNT can be thought as a bioreactor formed by $\text{Al}_2\text{Si}_2\text{O}_5(\text{OH})_4 \cdot 2\text{H}_2\text{O}$, where the Al is disposed in a gibbsite octahedral sheet (Al-OH) at the inner surface and siloxane (Si-O-Si) groups are exposed at the external surface. The interaction of the cationic polymer CTN occurs with the negative outer surface of the nanotube. CTN is absorbed on the outer surface of HNTs as a thin or thick-uniform layer depending on the mass ratio of the CTN to HNTs used in the preparation of the nanocomposite. The uniform-wrapping of biopolymer layer around nanotube has also been reported in other-biopolymer-nanotube hybrid systems¹⁴. The chemical composition of the CTN-HNTs (1:3) interface phase was analyzed by EDX spectroscopy and EDX spectrum is given in Fig. 4e. The chemical composition of the interface phase of CTN-HNTs was recorded as C(35.99%), N(4.48%), O(39.15%), Al(14.46%), Si(4.26%). As the chemical composition of pure HNTs was O(36.93%), Al(47.08%), Si(15.99%), the Al, Si and some part of the O belong to HNTs. The interface phase in the CTN-HNT nanocomposite consists of largely CTN and little HNTs. C and N are the characteristic elements of CTN. The remain part of the chemical composition came from gold-palladium using a sputter coated. When CTN come into close contact with HNTs, CTN is strongly suggested to be absorbed on the outersurface of HNTs. Therefore, the organic layer observed between HNTs and CTN interface is composed mainly of CTN.

TEM analysis

In TEM images, a light grey area extending through the HNTs show cylindrical open-ended interior lumen (Fig. 6 a). Pure CTN chains are absorbed on the surfaces, in pores and inner lumens of HNTs. CTN was proved to be absorbed on other

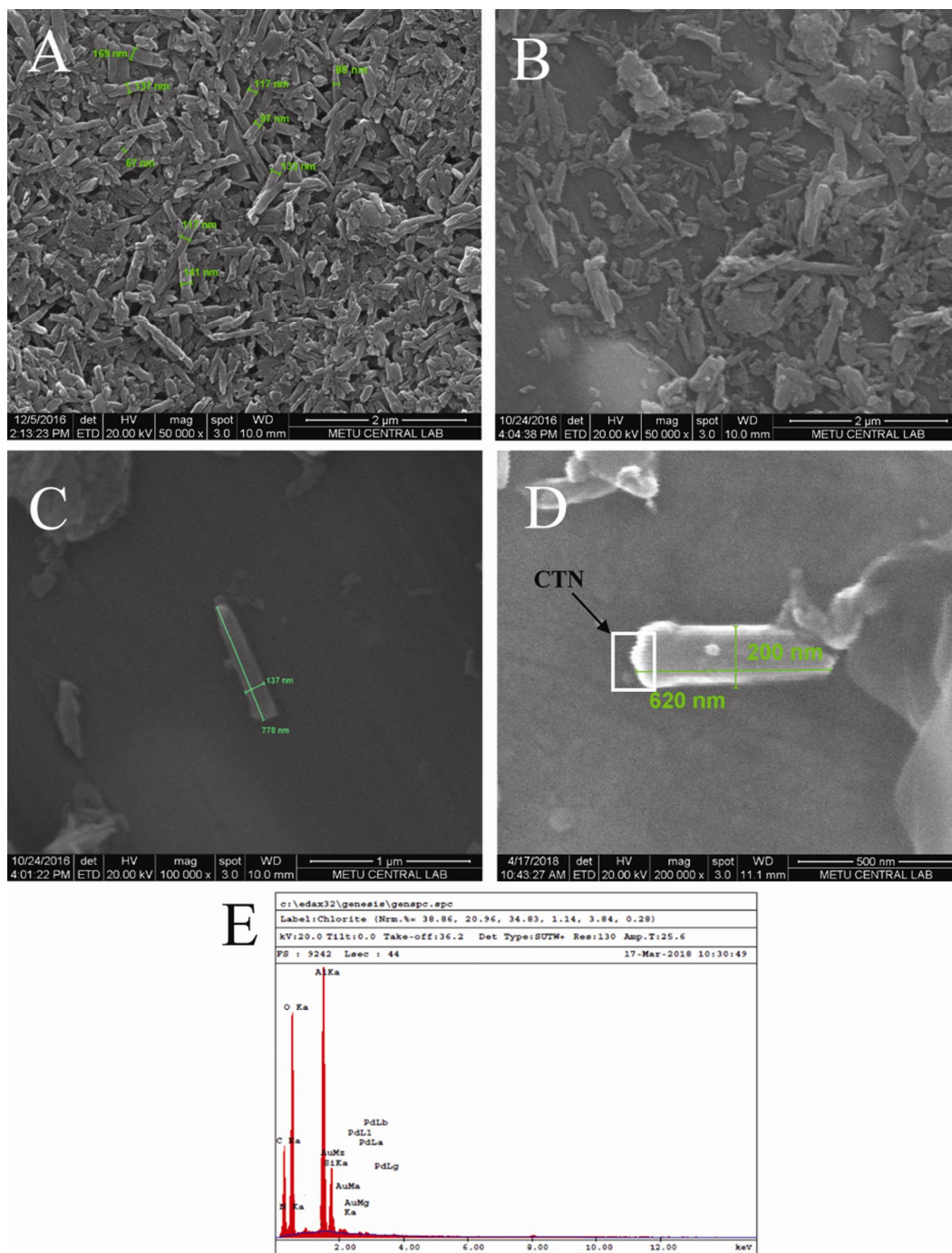


Fig. 5— SEM images of A) pure HNTs, B) CTN-HNT nanocomposites, C) diameter and length-labeled CTN-HNT nanocomposite, D) diameter and length-labeled CTN-HNT nanocomposite, the box indicates the location of the chitosan layer absorbed on the HNT, E-) EDX spectrum of the CTN-HNT interface phase.

silicate clays previously. The absorption behavior of CTN on HNTs was better observed in the TEM photos of the CTN-HNT nanocomposites. The edge of the CTN-HNT seems to be cloudy, unclear and blurry (Fig. 6b, c). A light gray organic layer was observed on the outer surfaces of the HNTs. As CTN phase is not electro

dense layer, it cannot be described in the TEM images. However, if the biopolymer layer is thick enough, it can be sighted. In TEM images, the lengths of CTN-HNT nanocomposites ranged from 500 nm to 750 nm. Size distributions determined by DLS measurements and SEM images were once again confirmed by TEM images.

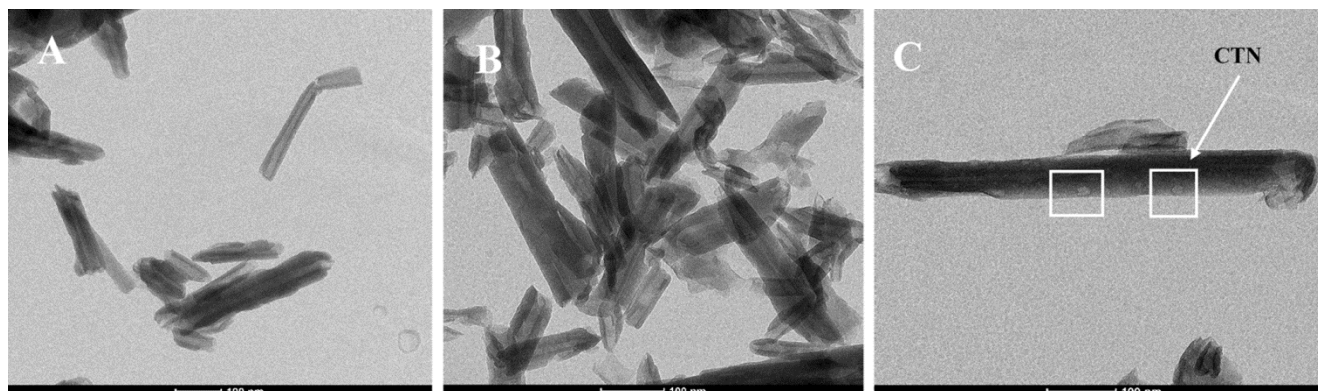


Fig. 6 — TEM images of A) pure HNTs B) CTN-HNT nanocomposites as bulk appearance, C) single nanocomposite, the box indicates the location of the chitosan layer adsorbed on the HNT.

BET measurements

The surface area of the CTN-HNT nanocomposites was determined by N_2 adsorption/desorption measurements with multipoint BET. Porous structure and high surface area are required to obtain high MNZ adsorption and loading. Surface areas of some clay-based nanoparticles were generally reported to decrease after modified by CTN. However, the surface area of the CTN-HNT nanocomposite was determined as $66.20 \text{ m}^2/\text{g}$, which is slightly higher than that of raw HNT ($65.80 \text{ m}^2/\text{g}$). The measured surface area showed that the nanopores of the CTN-HNT nanocomposite were suitable for the access of N_2 gas. The average pore diameter of the CTN-HNT nanocomposite was found to be 2.785 nm , and the pore volume was measured as $0.128 \text{ cm}^3/\text{g}$. Both of them are suitable for effective MNZ adsorption and for higher MNZ loading.

MNZ adsorption on CTN-HNT nanocomposites

Effects of pH and the mass ratio of HNT to CTN

The effect of pH on MNZ adsorption using 0.2 g of the CTN-HNT nanocomposite was investigated in 100 mL working volume and at 5 mg/L initial MNZ concentration. The CTN-HNT nanocomposites were prepared with different mass ratios of HNT to CTN of 1:1, 2:1, 3:1. At all mass ratios of HNT to CTN tested, the pH values of adsorption media were changed from 2.0 to 5.0.

CTN is positively charged in acidic solutions below pH 5.0 due to the protonation of amine groups. The HNTs are negatively charged at pH 2-13 due to the surface potential of SiO_2 with a small contribution from the positive Al_2O_3 inner surface. For that reason, mixing HNT with CTN in acidic aqueous medium results in electrostatic interactions between them. In addition, the amine groups and hydroxyl groups on

the CTN interact with the Si-O bonds of HNT through hydrogen bonding. The electrostatic interactions and hydrogen bonding between HNTs and CTN ensure interfacial binding which increase dispersion of the HNTs. MNZ can be found in aqueous solution in three different valencies with respect to medium pH. After complexation with CTN, the CTN-HNT nanocomposite can show a positive charge over the pH range of 3-9. However, when the mass ratio of HNT to CTN is increased to 3:1, the surface charge of CTN-HNT nanocomposite approximates to surface charge of HNTs. According to the MNZ speciation diagram, MNZ is positively charged in solution below pH 4.0, is the neutral in the pH range from 4.0 to 12.0, and is the anionic for pH greater than 12 (Ref 25). This suggests that the negatively charged CTN-HNT nanocomposites can adsorb MNZ via the electrostatic attraction interactions in the acidic aqueous solution.

In the Table 1, the initial MNZ adsorption rate, $r_i(\text{mg}/\text{g}\cdot\text{min})$, the amount of adsorbed MNZ per unit weight of CTN-HNT nanocomposite, $q_{\text{eq}}(\text{mg}/\text{g})$, the adsorbed MNZ concentration, $C_{\text{ads}}(\text{mg}/\text{L})$, and the adsorption efficiency, $Y_{\text{ads}}(\%)$, were compared at the different mass ratios of HNT to CTN of 1:1, 2:1, 3:1 and at pH values ranging from 2.0 to 5.0. The optimum mass ratio of HNT to CTN was decided to be 3/1. The maximum adsorption capacity, q_{eq} , and the adsorption efficiency, Y_{ads} , were obtained at 180 min of contact time, at pH 3.0 and were determined as $1.68 \text{ mg}/\text{g}$ and 66.14% , respectively.

The time-dependent change in the amounts of MNZ adsorbed per unit HNT-CTN weight for different mass ratios of HNT to CTN of 1:1, 2:1, 3:1 at pH 3.0 was given in Fig. 7. Initially MNZ adsorption occurred rapidly and a physical adsorption equilibrium was established between 30-120 mins,

Table 1 — For MNZ adsorption on CTN-HNT nanocomposite, comparison of initial adsorption rates, amount of MNZ adsorbed per unit weight of CTN-HNT nanocomposite, adsorbed MNZ concentration and adsorption efficiency obtained at different mass ratios of HNT to CTN and at pH values (amount of CTN-HNT nanocomposite: 0.2 g; initial MNZ concentration: 5 mg/L, T: 25°C).

	pH	r_i (mg/g.min)	q_{eq} (mg/g)	C_{ads} (mg/L)	Adsorption efficiency (%)
Mass ratio of HNT to CTN of 1/1	2	0.08	0.75	1.5	29.41
	3	0.32	1.02	2.05	41.16
	4	0.30	0.84	1.69	32.68
	5	0.02	0.63	1.26	25.14
Mass ratio of HNT to CTN of 2/1	pH	r_i (mg/g.min)	q_{eq} (mg/g)	C_{ads} (mg/L)	Adsorption efficiency (%)
	2	0.18	1.25	2.5	47.70
	3	0.55	1.09	2.18	41.92
	4	0.36	1.29	2.59	47.34
Mass ratio of HNT to CTN of 3/1	pH	r_i (mg/g.min)	q_{eq} (mg/g)	C_{ads} (mg/L)	Adsorption efficiency (%)
	2	0.14	1.61	3.22	63.13
	3	0.14	1.68	3.36	66.14
	4	0.136	1.4	2.8	56.56
	5	0.176	0.97	1.94	33.79

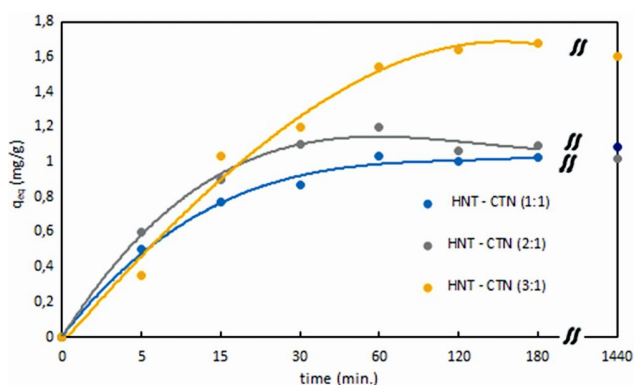


Fig. 7 — The time-dependent change in the amount of MNZ adsorbed per unit HNT-CTN weight at different mass ratios of HNT to CTN (pH 3.0; amount of CTN-HNT nanocomposite: 0.2 g, initial MNZ concentration: 5 mg/L; T= 25°C).

then the amount of MNZ adsorbed per unit HNT-CTN weight remained approximately constant until the end of 24 h. It was observed that the amount of MNZ adsorbed per unit HNT-CTN weight increased with the increasing mass ratio of HNT to CTN. The time-dependent change curve of the adsorption capacity of HNT-CTN 3/1 nanocomposite gave a steeply increasing slope.

Effect of the amount of CTN-HNT nanocomposite

The effect of the amount of CTN-HNT nanocomposite on MNZ adsorption using 0.1, 0.2, 0.4 and 0.8 g of the CTN-HNT nanocomposite was investigated in 100 mL working volume, at pH 3.0, at

the mass ratio of HNT to CTN 3/1 and at 5 mg/L initial MNZ concentration. When the amount of CTN-HNT nanocomposite was increased up to 0.2 g, the adsorbed MNZ concentration and the adsorption efficiency remained approximately constant and were determined as 3.51 mg/L, 69.43%, respectively. However, the amount of adsorbed MNZ per unit weight of CTN-HNT nanocomposite decreased (Fig. 8). For that reason, the optimum nanocomposite amount was determined as 0.2 g. At the higher amounts of CTN-HNT, the nanocomposites are proposed to be agglomerated and a decrease in active surface area is observed.

Effect of the MNZ concentration

To investigate the effect of MNZ concentration on MNZ adsorption, MNZ concentration using 0.2 g of the CTN-HNT nanocomposite in 100 mL working volume, at pH 3.0 and at the mass ratio of HNT to CTN 3/1 was increased from 5 to 50 mg/L. To prove the contribution of CTN for MNZ adsorption of the nanocomposite, the amount of adsorbed MNZ per unit weight of pure HNT was compared at increasing MNZ concentrations with that of the nanocomposite in Fig. 9. The initial MNZ adsorption rate, the adsorbed MNZ concentration and the amount of adsorbed MNZ per unit weight of CTN-HNT nanocomposite increased with increasing MNZ concentration and were determined as 0.268 mg/g –

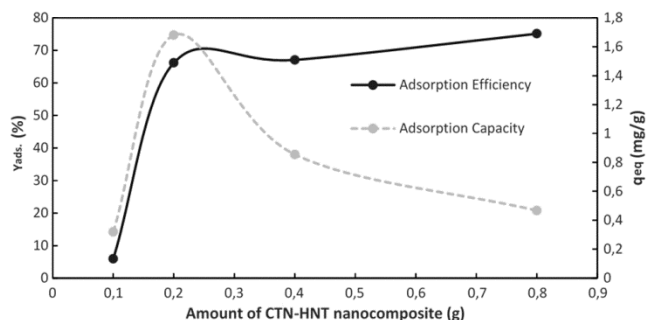


Fig. 8 — Effect of the amount of CTN-HNT nanocomposite on the amount of adsorbed MNZ per unit weight of CTN-HNT nanocomposite and adsorption efficiency (pH 3.0; initial MNZ concentration: 5 mg/L; mass ratio of HNT to CTN: 3/1, T= 25°C).

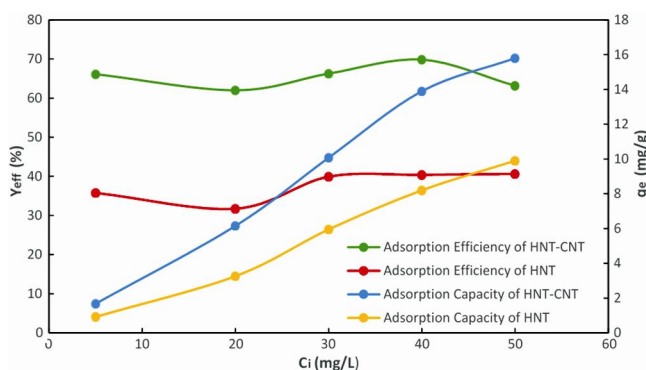


Fig. 9 — Effect of the initial concentration of MNZ on adsorption efficiency and the amount of adsorbed MNZ per unit weight of CTN-HNT nanocomposite and pure HNT (pH 3.0; amount of CTN-HNT nanocomposite: 0.2 g; amount of HNT: 0.2 g; mass ratio of HNT to CTN: 3/1, T= 25°C).

min, 31.6 mg/L, and 15.8 mg/g, respectively, at 50 mg/L initial MNZ concentration. The MNZ retention efficiency of CTN-HNT nanocomposite was remained approximately constant in the concentration range of 10-50 mg/L, and was determined as 62.01-69.84%, respectively. The maximum initial MNZ adsorption rate, the adsorbed MNZ concentration and the amount of adsorbed MNZ per unit weight of pure HNT were obtained as 1.916 mg/g – min, 19.8 mg/L, 9.9 mg/g, respectively, at 50 mg/L initial MNZ concentration. The maximum MNZ adsorption efficiency of pure HNT was detected as approximately 40% in the concentration range of 30-50 mg/L. It was observed that the MNZ adsorption capacity significantly increased with the addition of CTN in a 3: 1 ratio to the nanocomposite structure compared to pure HNT.

Equilibrium models for MNZ adsorption on CTN-HNT nanocomposite

The Langmuir and Freundlich adsorption equilibrium models were fitted to the experimental

Table 2 — Langmuir Model constants for MNZ adsorption on CTN-HNT nanocomposite (pH 3.0; amount of CTN-HNT nanocomposite: 0.2 g; mass ratio of HNT to CTN: 3/1, T: 25°C).

q_m (mg/g)	b (L/mg)	a (L/g)	R^2	MRE (%)
23.321	0.045	1.049	0.990	9.20

Table 3 — Freundlich Model constants for MNZ adsorption on CTN-HNT nanocomposite (pH 3.0; amount of CTN-HNT nanocomposite: 0.2 g; mass ratio of HNT to CTN: 3/1, T: 25°C).

$K_F(\text{mg}^{(1-1/n)}/\text{g} \cdot \text{L}^n)$	$1/n$	n	R^2	MRE (%)
1.150	0.781	1.280	0.942	11.83

MNZ adsorption equilibrium data on CTN-HNT nanocomposite. The Langmuir equation given by Eqn. (1) is the most widely used isotherm equation for modelling adsorption equilibrium data²⁶:

$$q_e = \frac{a \cdot C_{eq}}{1 + b \cdot C_{eq}} \quad \dots(1)$$

where C_{eq} is the unadsorbed MNZ concentration at equilibrium in solution and $a = q_m \cdot b$. q_m is the amount of MNZ adsorbed per unit weight of CTN-HNT nanocomposite at equilibrium to form a complete monolayer on the surface and b is the adsorption equilibrium constant or the ratio of adsorption/desorption rates.

$$= \frac{b}{a} + \frac{1}{a \cdot C_{eq}} \quad \dots(2)$$

Therefore, a plot of $1/q_{eq}$ vs. $1/C_{eq}$ gives a straight line of slope $1/a$ and intercept b/a (Table 2).

The Freundlich equation is commonly presented as²⁷:

$$= K_F \cdot C_{eq}^{1/n} \quad \dots(3)$$

This nonlinear equation is linearized to determine the Freundlich constants from the slope and intercept,

$$\ln q_e = \ln K_F + 1/n \ln C_{eq} \quad \dots(4)$$

which are equal to $1/n$ and $\ln K_F$ at $C_{eq} = 1.0$, respectively. Magnitude of K_F is an indication of MNZ adsorption capacity of the CTN-HNT nanocomposite, the slope $1/n$ represents the adsorption intensity. If adsorption is favourable, then $1/n < 1$ or $n > 1$ (Table 3).

A further empirical isotherm developed by Redlich and Peterson incorporated three parameters (Redlich and Peterson):

$$= \frac{K_R \cdot C_e}{1 + a_R \cdot C_e^\beta} \quad \dots(5)$$

where the exponent β lies 0 and 1. When $\beta = 1$, the Redlich-Peterson equation reduces to the Langmuir

equation. If $a_R C_{eq}^\beta$ is much greater than 1, then it becomes the Freundlich equation. If $a_R C_{eq}^\beta$ is much less than 1, which occurs at low concentrations, then it becomes a linear isotherm equation and the Henry's Law form results. The Redlich-Peterson model constants were calculated using the solver add-in for Microsoft Excel 2016 computer program with non-linear regression (Table 4).

The adsorption isotherms for MNZ adsorption on CTN-HNT nanocomposite are given in Fig. 10. The Langmuir, Freundlich and Redlich-Peterson model profiles are presented in full, dashed and dot lines, respectively, whereas the symbols show experimentally obtained values. The MNZ adsorption on CTN-HNT nanocomposite was represented better by the Langmuir model than by the Freundlich and Redlich-Peterson models, since both the regression coefficients and the percent mean relative error (MRE %) values were found to be better compared to other models. This result propose that the surface has a specific number of sites where the MNZ molecules can be adsorbed. It is also suggested that the adsorption involves the attachment of only one layer of MNZ molecules to the surface. The Freundlich model generally agrees well with the Langmuir model and experimental data over moderate ranges of concentration: both of them are characteristic of adsorption from aqueous solutions. On the other hand, the approximation of the value of the β constant to 1

pointed out that the Redlich-Peterson model can be reduced to the Langmuir model. The K_R value calculated from the Redlich-Peterson model also approximated to the q_m value found from the Langmuir model. This was also once again verified that the Langmuir Model is the best adsorption model to represent the MNZ adsorption equilibrium data on halloysite nanotubes.

Kinetic models for MNZ adsorption on CTN-HNT nanocomposite

In order to explain the kinetic mechanism of MNZ adsorption on CTN-HNT nanocomposites, the pseudo-first order model of Lagergren²⁸ and the pseudo-second-order model of Ho and McKay²⁹ were used. The linearized forms of pseudo-first and second-order models are presented as follows:

$$\text{Pseudo-first order: } (q_t - q_{eq}) = (q_{eq} - q_0) e^{-k_1 t} \quad \dots(6)$$

$$\text{Pseudo-second order: } \frac{t}{q_t} = \frac{1}{k_2 q_{eq}^2} + \frac{1}{q_{eq}} t \quad \dots(7)$$

where q_t is the amount of MNZ adsorbed per unit weight of CTN-HNT nanocomposite at any time t , q_{eq} the amount of MNZ adsorbed per unit weight of CTN-HNT nanocomposite at equilibrium, k_1 is the pseudo-first-order rate constant, k_2 the pseudo-second-order rate constant. The linearized equations for these models along with the regression coefficients are given in Table 5. The adsorption kinetics of MNZ on CTN-HNT nanocomposite is better characterized by the pseudo-first-order model than by the pseudo-second-order model with correlation coefficients ranging from 0.906 – 0.991. The one-site models are the first-order models. The adsorption rate is proposed to be limited by only one process or mechanism on a single class of sorbing sites. When the initial MNZ dosage is increased, the longer time is required to attain an adsorption equilibrium. For that reason, when the initial MNZ concentrations are increased, the values of pseudo-first order rate constants are expected to decrease, as also observed.

The amounts of MNZ adsorbed per unit surface area of CTN-HNT nanocomposite are given in Table 6. When the initial MNZ concentrations were increased, the amount of MNZ adsorbed per unit surface area of CTN-HNT nanocomposite increased up to 30 mg/L, then remained approximately constant. It was seen that the surface of CTN-HNT nanocomposite became saturated with MNZ at higher concentrations than 30 mg/L.

Table 4 — Redlich - Peterson Model constants for MNZ adsorption on CTN-HNT nanocomposite (pH 3.0; amount of CTN-HNT nanocomposite: 0.2 g; mass ratio of HNT to CTN: 3/1, T: 25°C).

K_R (L/g)	a_R ($\text{mg}^{\beta+1}/\text{g} \cdot \text{L}^\beta$)	β	SSE	MRE (%)
0.930	0.036	0.90	33.57	13.62

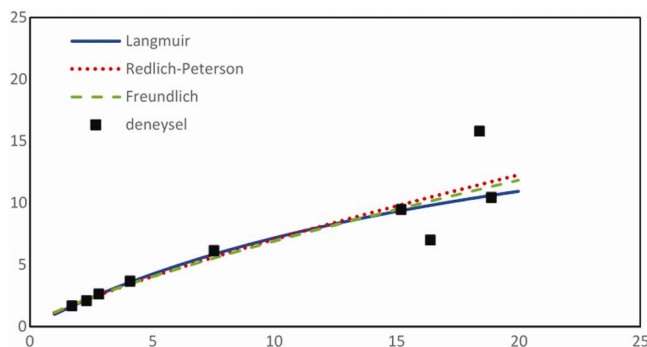


Fig. 10 — Comparison of Langmuir, Freundlich and Redlich-Peterson adsorption models for MNZ adsorption on CTN-HNT nanocomposite (pH 3.0; amount of CTN-HNT nanocomposite: 0.2 g; mass ratio of HNT to CTN: 3/1, T= 25°C).

Table 5 — Comparison of pseudo-first-order and second-order rate models and correlation coefficients for MNZ adsorption on CTN-HNT nanocomposite (pH 3.0; amount of CTN-HNT nanocomposite: 0.2 g; mass ratio of HNT to CTN: 3/1, T: 25°C).

MNZ concentration (mg/L)	Pseudo First Order Rate Equation	R ²
5.4	$\ln(q_{eq} - q_t) = 0.258 - 0.071t$	0.966
19.85	$\ln(q_{eq} - q_t) = 1.797 - 0.043t$	0.991
30.4	$\ln(q_{eq} - q_t) = 2.261 - 0.022t$	0.967
39.8	$\ln(q_{eq} - q_t) = 2.578 - 0.024t$	0.970
50.01	$\ln(q_{eq} - q_t) = 2.636 - 0.027t$	0.906
MNZ concentration (mg/L)	Pseudo Second Order Rate Equation	R ²
5.4	$\frac{t}{q_t} = 6.184 + 0.562t$	0.980
19.85	$\frac{t}{q_t} = 6.135 + 0.136t$	0.770
30.4	$\frac{t}{q_t} = 8.897 + 0.094t$	0.780
39.8	$\frac{t}{q_t} = 9.360 + 0.058t$	0.840
50.01	$\frac{t}{q_t} = 9.079 + 0.055t$	0.920

Table 6 — The amounts of MNZ adsorbed per unit surface area of CTN-HNT nanocomposite at increasing MNZ concentrations (pH 3.0; amount of CTN-HNT nanocomposite: 0.2 g; mass ratio of HNT to CTN: 3/1, T: 25°C).

Initial MNZ concentrations (mg/L)	Amount of MNZ adsorbed per unit surface area of CTN-HNT (mg/m ²)
5	0.025
10	0.092
20	0.152
30	0.209
50	0.238

MNZ loading to CTN-HNT nanocomposite

Using the calibration line of MNZ in PBS buffer, the amount of free MNZ in 2mL of buffer solution was determined and this value was subtracted from the amount of added total drug. In this way, the MNZ amount encapsulated by CTN-HNT nanocomposite in PBS buffer was calculated using Eqn. (8)³⁰.

$$\text{Encapsulation Efficiency (\%)} = \frac{\text{total amount of drug added} - \text{free drug}}{\text{total amount of drug added}} \times 100 \quad \dots(8)$$

The encapsulation efficiency of MNZ in PBS buffer was found as 67.0%. The MNZ adsorption efficiency of CTN-HNT nanocomposite was found to be approximately constant in the concentration range

of 10 mg/L –50 mg/L (Fig. 9). In this MNZ concentration range, the average MNZ adsorption efficiency was determined as 65.5%. The encapsulation efficiency of MNZ was found to be very close to the MNZ loading via adsorption. This demonstrated the success of MNZ immobilization in CTN-HNT nanocomposites by both direct loading and adsorption method. It was also verified that the MNZ saturation retention capacity of the CTN-HNT nanocomposite was approximately the same.

In addition, the drug loading capacity per the amount of MNZ loaded CTN-HNT nanocomposite in PBS buffer was calculated using Eqn. (9).

$$\text{g Loading capacity (\%)} = \frac{\text{total amount of drug added} - \text{free drug}}{\text{total amount of composite} + \text{total amount of drug added}} \times 100 \quad \dots(9)$$

The MNZ loading capacity was obtained as 4.36%.

MNZ release from CTN-HNT nanocomposite

When 0.5 g of MNZ was loaded to the CTN-HNT nanocomposites, MNZ release studies were carried out at different pH conditions corresponding to the gastric and intestinal media at 37°C. Time-dependent *in-vitro* MNZ release profile from CTN-HNT nanocomposite was obtained in HCl buffer solution at pH 1.2 and 0.1 M PBS at pH 7.4. The MNZ release from CTN-HNT nanocomposites was calculated using Eqn. (10).

$$\text{g Release (\%)} = \frac{R_t}{L} \times 100 \quad \dots(10)$$

R_t: Cumulative amount of drug released at time t (mg)

L: Initial amount of drug (mg)

To prevent gastric distress and increase the medical effectiveness, high and rapid release of MNZ would be better to occur in the intestine instead of in the stomach. A release burst occurred within 6 h of CTN-HNT-MNZ in simulated gastric medium and displayed 42.86 wt% of MNZ in the initial release stage. The release process of CTN-HNT-MNZ continued to increase at a slower rate from 6 h to 14 h with 49.58 wt% of MNZ. After the initial burst, there was a steady rise of MNZ release until 20 h to reach 52.10 wt% (Fig. 11 a).

CTN-HNT-MNZ system also showed the release burst within 6 h in the simulated intestinal fluid and reached 56.35% release of MNZ, which was followed the lower release amount of MNZ from 6 h to 10 h and reached 62.0%. Then the drug release reached a plateau after 10 h, a sustained and long-term release profile was observed until 20 h with a MNZ release of

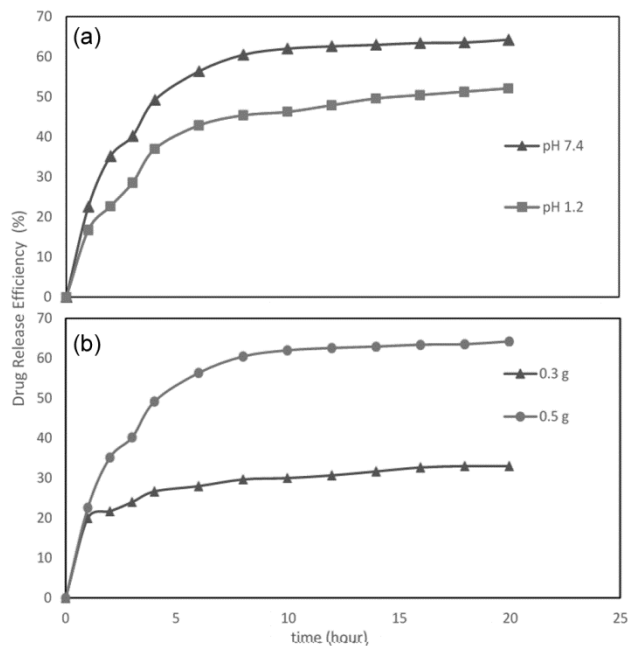


Fig. 11 — Time-dependent in-vitro release profiles of MNZ from CTN-HNT nanocomposite a-) in HCl at pH 1.2 and PBS buffer solution at 7.4 at 37°C when 0.5 g of MNZ was loaded, b-) when the loaded MNZ was increased from 0.3 g to 0.5 g in PBS buffer solution.

64.23 wt%. In the CTN-HNT-MNZ release system, more rapid release rate and higher release amount of MNZ in the simulated intestinal medium where as the lower release amount in the simulated gastric medium are desired to keep effective concentration of MNZ in the body and decrease the maximum extent of the side effects to the stomach.

When the loaded MNZ was increased from 0.3 to 0.5 g, the MNZ release also enhanced from 33.0 to 64.23% of the loaded MNZ in PBS at the end of 20 h. (Fig. 11 b-).

The effect of mass ratio of HNT to CTN of 2:1, 3:1 on release of MNZ was investigated both in HCl buffer solution at pH 1.2 and 0.1 M PBS at pH 7.4, and compared with pure HNT. When the mass ratio of HNT to CTN was chosen as 3:1 and 2:1 in HCl buffer solution, the MNZ release increased from 35.46 to 52.10% at the end of 20 h. In the same buffer solution a MNZ release of 30.05% was obtained from pure HNT (Fig. 12 a). In the 0.1 M PBS, the MNZ releases also increased with increasing mass ratio of HNT to CTN of 3:1, 2:1, and were detected as 48.23%, 64.23%, respectively. The MNZ release of pure HNT in PBS buffer solution was found to be 40.29% (Fig. 12 b). Higher MNZ release was observed with increasing mass ratio of HNT to CTN which could be

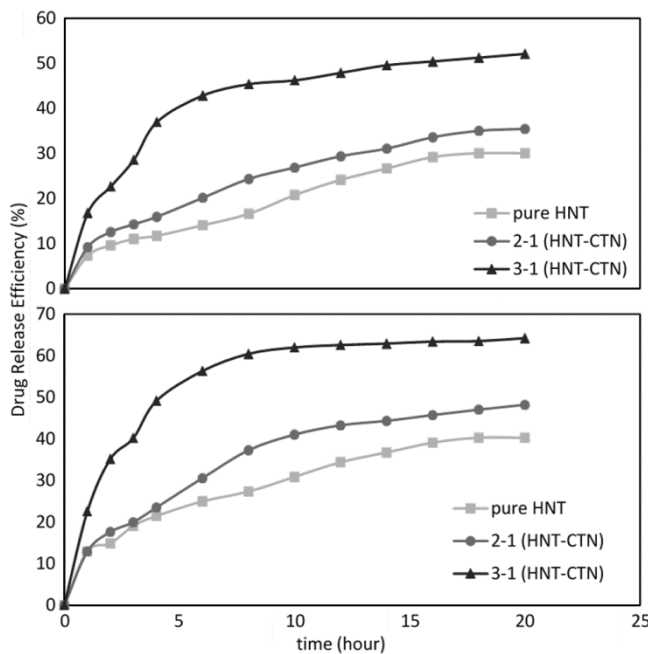


Fig. 12 — Time-dependent in-vitro release profiles of MNZ from pure HNT and CTN-HNT nanocomposite at different mass ratios of HNT to CTN a-) in HCl at pH 1.2 and b-) PBS buffer solution at 7.4 at 37°C when 0.5 g of MNZ was loaded.

related to the opposite charges between lumens and surfaces of HNTs. The electrostatic repulsion of MNZ due to surface charge of HNT-CTN nanocomposite with changing medium pH accelerated the release of MNZ from the nanocomposite leading the higher release rate.

Conclusion

In the present study, the MNZ adsorption capacity of CTN-HNT nanocomposites and potential of the nanocomposites as MNZ carriers for controlled MNZ delivery were investigated. The maximum initial MNZ adsorption rate, the adsorption capacity and efficiency of CTN-HNT nanocomposite were found to be 0.268 mg/g-min, 15.8 mg/g and 63.19%, respectively. The fit of MNZ adsorption equilibrium on CTN-HNT nanocomposites to the Langmuir and Freundlich models was investigated, and a good agreement was generally observed in both the models at moderate concentration levels of MNZ. The encapsulation efficiency of MNZ in PBS buffer was found to be 67%, this value is very close to the MNZ loading (65.5%) via adsorption. When 0.5 g MNZ was loaded to CTN-HNT, a sustained and long-term release profile was observed until 20 h with a MNZ release of 64.23 wt% in PBS buffer. Slow drug release demonstrates a controlled,

prolonged route for MNZ diffusing through the polymer-clay network.

Acknowledgement

The authors wish to thank H.U. BAP (Hacettepe University Scientific Research Projects Coordination Unit) for financial support of this study (project no: 014 01 602 001-523) and TUBITAK, the Scientific and Technical Research Council of Turkey with 2210-C programme. The authors also wish to thank Middle East Technical University Central Laboratory for the particle size distribution, SEM, TEM, BET measurements of the CTN-HNT nanocomposites.

References

- 1 Elieh-Ali-Komi D & Hamblin M R, *Int J Adv Res*, 4 (2016) 411.
- 2 Rinaudo M, *Prog Polym Sci*, 2006, 603.
- 3 Goze B, Evirgen O A & Acikel Y S, *Desalin Water Treat*, 57 (2016) 4059.
- 4 Hussain M R & Maji T K, *J Microencapsul*, 25 (2008) 414.
- 5 Khalil H, Saurabh C K, Adnan A S, Fazita M R N, Syakir M I, Davoudpour Y, Rafatullah M, Abdullah C K, Haafiz M K M & Dungani R, *Carbohydr Polym*, 150 (2016) 216.
- 6 Liu M X, Zhang Y, Wu C C, Xiong S & Zhou C R, *Int J Biol Macromol*, 51 (2012) 566.
- 7 Liu M X, Guo B C, Zou Q L, Du M L & Jia D, *Nanotechnology*, 19 (2008) 10.
- 8 Liu M X, Wu C C, Jiao Y P, Xiong S & Zhou C R, *J Mat Chem B*, 1(2013) 2078.
- 9 Yuan P, Thill A & Bergaya F, *Developments in Clay Science*, 7th edn, (Elsevier) 2016.
- 10 Lvov Y, Wang W, Zhang L & Fakhrullin R, *Adv Mater*, 28 (2016) 1227.
- 11 Cavallaro G, Lazzara G, Milioto S, Parisi F, Evtugyn V, Rozhina E & Fakhrullin R, *ACS Appl Mater Interfaces*, 10 (2018) 8265.
- 12 Bertolino V, Cavallaro G, Lazzara G, Milioto S & Parisi F, *Langmuir*, 33 (2017) 3317.
- 13 Makaremi M, Pasbakhsh P, Cavallaro G, Lazzara G, Aw Y K, Lee S M & Milioto S, *ACS Appl Mater Interfaces*, 9 (2017) 17476.
- 14 Bertolino V, Cavallaro G, Merli M, Milioto S, Parisi F & Sciascia L, *Ind Eng Chem Res*, 55 (2016) 7373.
- 15 Zhai R, Zhang B, Wan Y Z, Li C C, Wang J T, Liu J D, *Chem Eng J*, 214 (2013) 304.
- 16 Canales-Alvarado D H, Ocampo-Perez R, Leyva-Ramos R & Rivera-Utrilla J, *J Colloid Interface Sci*, 436 (2014) 276.
- 17 Song Q S, Pruckler J, Fields P, Swaminathan B & Gold B D, *Gastroenterology*, 124 (2003) A405.
- 18 Viseras C, Aguzzi C, Cerezo P & Bedmar M C, *Mater Sci Technol*, 24 (2008) 1020.
- 19 Shaikh R, Raj Singh T R, Garland M J, Woolfson A D & Donnelly R F, *J Pharm Bioallied Sci*, 3 (2011) 89.
- 20 Bugatti V, Viscusi G, Naddeo C & Gorrasi G, *Nanomater*, 7 (2017) 12.
- 21 Eizatahry A A & Eldin M S M, *Polym Adv Technol*, 19 (2008) 1787.
- 22 Abou-Shoer M, *Am J Anal Chem*, 1 (2010) 91.
- 23 De Silva R T, Pasbakhsh P, Goh K L, Chai S P & Ismail H, *Polym Test*, 32 (2013) 265.
- 24 Liu M X, Zhang Y, Li J J & Zhou C R, *Int J Biol Macromol*, 58 (2013) 23.
- 25 Rivera-Utrilla J, Prados-Joya G, Sanchez-Polo M, Ferro-Garcia M A & Bautista-Toledo I, *J Hazard Mater*, 170 (2009) 298.
- 26 Langmuir I, *J Am Chem Soc*, 38 (1916) 2221.
- 27 Freundlich H, *Zeitschrift fr Physikalische Chemie*, 57A (1907) 385.
- 28 Lagergren S, *Handlingar*, 24 4) (1898) 1.
- 29 Ho Y S & McKay G, *Process Biochem*, 34 (1999) 451.
- 30 Pichayakorn W & Boonme P, *Mater Sci Eng C-Mater Biol Appl*, 33 (2013) 1197.